Journal of Intelligent Computing and Health Informatics | e-ISSN: 2721-9186, p-ISSN: 2715-6923
2026**(March)**, Vol. 7, No. 1, 1–17, https://doi.org/10.26714/jichi.v7i1.19802
Official Site: https://jurnal.unimus.ac.id/index.php/ICHI

Research Article

High precision cascaded spatio temporal deep inference for real time histamine risk prediction: A health informatics approach

Hanityo Adi Nugroho[1,*], Dorojatun AN[2], Rubijanto Juni Pribadi[3], and Samsudi Raharjo[3]

[1]*Department of Marine Science, Faculty of Science and Agriculture Technology, Universitas Muhammadiyah Semarang, Semarang 50273, Indonesia*
[2]*Department of Postgraduate Studies, Energy Conversion Engineering, Faculty of Mechanical Engineering, Universitas Brawijaya, Malang 65145, Indonesia*
[3]*Mechanical Engineering, Faculty of Engineering and Computer Science, Universitas Muhammadiyah Semarang, Semarang 50273, Indonesia*

***Correspondence:** Hanityo Adi Nugroho hanityoadi@unimus.ac.id

Received: 3 December 2025; Revised: 15 January 2026; Accepted: 19 March 2026, Published: 31 March 2026

ABSTRACT

Rapid histamine accumulation in tropical fisheries constitutes a substantial public health hazard, particularly via scombroid poisoning, and underscores the need for rigorous, data-driven cold-chain surveillance. Artisanal vessels ($\leq$ 30 GT), however, predominantly depend on ice-based cooling strategies that are thermally unstable and lack real-time diagnostic functionality, thereby failing to sufficiently suppress microbial growth kinetics under ambient conditions that frequently exceed 30 °C. To address this gap, we propose a Cascaded Spatio-Temporal Deep Inference Architecture that couples a Convolutional Neural Network (CNN) for spatial feature denoising with a Long Short-Term Memory (LSTM) network for temporal kinetic modeling. This hybrid architecture assimilates high-frequency thermal measurements from an optimized R404A vapor-compression refrigeration system and predicts histamine risk indices under Arrhenius-based kinetic constraints. Field deployment on a 10 GT vessel demonstrated that the system maintained a highly stable storage temperature of -20.1 ± 0.5 °C. The proposed model exhibited high predictive accuracy with an R^2 of 0.97 and an RMSE of 0.45 °C, significantly outperforming a Linear Regression baseline (RMSE $= 1.85$ °C, $p < 0.01$). Importantly, the system extended the prime-quality shelf life by more than 52 hours while keeping histamine concentrations well below the U.S. FDA limit of 50 mg/kg. Collectively, these findings support a scalable health informatics framework and indicate that AI-driven predictive certification can substantially reduce food safety risks in resource-limited maritime supply chains.

KEYWORDS

Scombroid Poisoning; Cold Chain Monitoring; Hybrid CNN-LSTM; Histamine Prediction; Health Informatics; R404A Refrigeration

1. Introduction

The integrity of the global seafood supply chain constitutes a fundamental determinant of food security and a critical domain of inquiry within public health informatics. Scombroid fish species, such as skipjack (*Katsuwonus pelamis*), exhibit a pronounced susceptibility to the rapid formation of biogenic amines, predominantly histamine, when subjected to thermal abuse during the post-harvest phase [1, 2]. Histamine intoxication, clinically recognized as scombroid poisoning, remains a widespread foodborne hazard worldwide, with disproportionate impact on vulnerable population groups [3, 4]. In tropical archipelagic regions, ambient temperatures that frequently exceed 30°C markedly accelerate microbial growth kinetics, thereby necessitating an exceptionally robust and continuously maintained cold chain from the point of capture onward [5, 6].

To address these thermal vulnerabilities, recent engineering efforts have centered on advanced thermal insulation materials and optimized active refrigeration strategies. Zhang et al. [7] demonstrated that the incorporation of Phase Change Materials (PCM) into polyurethane foam can substantially enhance thermal inertia, while Duan et al. [8] provided a comprehensive review of the deployment of such thermal energy storage solutions in transport logistics. In parallel, progress in active cooling technologies has been reported by Maiolo et al. [9] and Sun et al. [10], who investigated vapor-compression refrigeration architectures and alternative refrigerants to improve the energetic performance of mobile cold storage systems. Nonetheless, mechanical and material improvements alone are insufficient in the absence of real-time predictive and diagnostic capabilities. Current FDA regulations underscore that safeguarding food safety requires continuous acquisition and analysis of time–temperature profiles to effectively constrain pathogen proliferation [11].

Emerging paradigms in intelligent systems have sought to close this methodological and operational gap through the integration of the Internet of Things (IoT) with Machine Learning (ML). Prior studies by Tsironi et al. [12] and Alfian et al. [13] employed regression-based predictive models coupled with real-time sensor networks to estimate product freshness. Within the Deep Learning domain, Han et al. [14] successfully implemented Long Short-Term Memory (LSTM) architectures to forecast temperature dynamics in refrigerated containers, whereas Wang et al. [15] applied Recurrent Neural Networks (RNN) to detect disruptions in the cold chain by leveraging spectral signal profiles. Despite these advances, a substantial technical gap remains in the current State-of-the-Art (SOTA). Specifically, conventional statistical approaches and standard Artificial Neural Networks (ANN) exhibit limited capacity to model the high-dimensional, strongly non-linear, and temporally coupled dependencies that characterize operational conditions in tropical small-scale fisheries.

Standard Convolutional Neural Networks (CNNs) are highly effective for spatial feature extraction; however, they inherently lack the temporal memory capacity necessary to accurately characterize the cumulative kinetics of bacterial proliferation as described by Boonsumrej and Chaiyapech [16]. In contrast, standalone Long Short-Term Memory (LSTM) networks, although well-suited for time-series modeling, exhibit reduced robustness to thermal noise and abrupt spatial perturbations, such as rapid heat ingress during frequent hatch openings, that are characteristic of artisanal refrigeration vessel operations [17]. Moreover, the prevailing body of literature typically considers thermodynamic refrigeration efficiency and microbiological/clinical risk as largely independent domains, thereby creating a gap for an integrated, real-time forecasting paradigm that explicitly links mechanical refrigeration performance to resultant clinical safety outcomes [18].

To address these limitations, this study introduces an AI-driven Health Informatics Framework that systematically integrates optimized refrigeration thermodynamics with predictive microbiological safety modeling. We develop a Hybrid LSTM–CNN architecture tailored for multivariate time-series analysis of histamine formation. In this configuration, the CNN module functions analogously to a high-pass filter, extracting salient spatio-temporal features from volatile sensor streams, while the LSTM module captures long-range temporal dependencies governed by Arrhenius–Schöner-type kinetic behavior. Utilizing high-resolution thermal data derived from an optimized R404A–polyurethane (PU) refrigeration system, the proposed framework formulates a "Thermal Inertia" model that substantially improves predictive robustness under highly variable, tropical environmental conditions.

The principal technical contributions of this study are summarized as follows: (1) We introduce a multilayer deep learning architecture that concurrently models spatial thermal spike patterns and temporal microbial dynamics, mitigating the vanishing-gradient phenomena associated with single-stream architectures; (2) We develop a rigorous mathematical framework that couples R404A-optimized thermodynamic descriptors with real-time biogenic amine (BA) accumulation profiles; and (3) We demonstrate, through systematic benchmarking, that the proposed framework yields substantial reductions in Mean Absolute Error (MAE) and Root Mean Square Error (RMSE), furnishing robust early-warning indicators of histamine hazards under

extreme tropical thermal stress.

The remainder of this paper is structured as follows. Section 2 introduces the necessary preliminaries, including the formal mathematical notation underlying the LSTM–CNN framework and the kinetics of biogenic amines. Section 3 describes the proposed methodology and the corresponding system architecture in detail. Section 4 reports the experimental results, together with statistical validation based on the Wilcoxon signed-rank test, and provides an extensive discussion of the findings. Finally, Section 5 summarizes the main conclusions of the study and delineates potential avenues for future research.

2. Preliminaries

This section establishes the formal theoretical foundation and mathematical rigor required to comprehend the proposed hybrid informatics framework. We define the fundamental notations, the kinetics of biogenic amine degradation, and the baseline deep learning architectures used as the benchmark for real-time risk prediction.

2.1. Table of Notations

To ensure consistency throughout the manuscript, the primary mathematical symbols and operators are defined in Table 1.

Table 1. Formal mathematical notations and symbols.

Symbol	Definition	Unit/Domain
$\mathcal{T}$	Time-series temperature vector from R404A sensors	$^{\circ}$C
$C(t)$	Concentration of histamine at time t	mg/kg
$k(T)$	Temperature-dependent reaction rate constant	h^{-1}
E_a	Activation energy for microbial decarboxylation	$J \cdot mol^{-1}$
$\mathbf{X}$	Input feature matrix for the CNN layer	$\mathbb{R}^{n \times m}$
$\mathbf{w}$	Convolutional filter kernel (learnable weights)	$\mathbb{R}^{k \times k}$
f_t, i_t, o_t	LSTM gates: Forget, Input, and Output gates	$[0, 1]$
C_t, h_t	LSTM cell state and hidden state (internal memory)	$\mathbb{R}^d$
$\odot$	Hadamard (element-wise) product operator	–
HRI	Normalized Health Risk Index	$[0, \infty)$

2.2. Thermodynamic Modeling of Biogenic Amine Kinetics

The formation of histamine in scombroid species is a dynamic biochemical process driven by the microbial decarboxylation of L-histidine. We formalize this using integrated kinetic models.

2.2.1 General Order Kinetic Formulation

The rate of histamine accumulation dC/dt is modeled as a function of the remaining capacity for spoilage, defined as follows:

$$\frac{dC}{dt} = k(T) \cdot [C_{\text{max}} - C(t)]^n \tag{1}$$

where C_{max} represents the theoretical saturation point of histamine under tropical ambient conditions and n denotes the reaction order, typically assumed as first-order ($n = 1$) for microbial kinetics in scombroid fish [16]. This kinetic approach aligns with recent cold chain management improvements described by Qian et al. [19], which emphasize the shift from static quality checks to dynamic, process-based monitoring.

2.2.2 Arrhenius-Schoener Temperature Dependency

To map the influence of R404A storage fluctuations on microbial activity, the rate constant $k(T)$ is governed by the Arrhenius law [20]:

$$k(T) = A \cdot \exp\left(-\frac{E_a}{R \cdot T(t)}\right) \tag{2}$$

where A is the pre-exponential frequency factor and R is the universal gas constant ($8.314\,\mathrm{J}\cdot\mathrm{mol}^{-1}\cdot\mathrm{K}^{-1}$). This equation establishes the "Biological Benchmark" that our AI model seeks to approximate through deep learning.

2.3. Deep Learning Foundations for High-Dimensional Time-Series

The proposed framework utilizes two distinct neural mechanisms to process the non-linear thermal noise of artisanal fishing voyages. As highlighted in the comprehensive review by Ismail Fawaz et al. [21], deep learning architectures demonstrate superior performance in classifying and forecasting multivariate time-series data compared to traditional distance-based methods.

2.3.1 Convolutional Operators for Spatial Feature Denoising

Convolutional Neural Networks (CNN) are utilized to extract salient features from sudden thermal spikes. Let $\mathbf{X}$ be the input matrix; the transformation to a feature map $y_{i,j}$ is defined by:

$$y_{i,j} = \mathrm{ReLU}\left(\sum_{m}\sum_{n} \mathbf{w}_{m,n}\cdot x_{i+m,j+n} + b\right) \tag{3}$$

The ReLU activation function ensures that the model ignores negative-value noise, focusing only on significant positive thermal gradients caused by hatch openings or refrigeration failure. This specific application of CNN for noise reduction in logistics has been corroborated by recent studies in cold chain intelligence [15].

2.3.2 Long Short-Term Memory for Temporal Microbial Dependencies

To address the vanishing gradient problem in long-duration (120-hour) voyages, the LSTM unit maintains a persistent cell state C_t. The information flow is regulated by the following gating system:

$$f_t = \sigma(\mathbf{W}_f \cdot [\mathbf{h}_{t-1}, \mathbf{x}_t] + \mathbf{b}_f) \tag{4}$$
$$i_t = \sigma(\mathbf{W}_i \cdot [\mathbf{h}_{t-1}, \mathbf{x}_t] + \mathbf{b}_i) \tag{5}$$
$$\tilde{C}_t = \tanh(\mathbf{W}_C \cdot [\mathbf{h}_{t-1}, \mathbf{x}_t] + \mathbf{b}_C) \tag{6}$$
$$C_t = f_t \odot C_{t-1} + i_t \odot \tilde{C}_t \tag{7}$$
$$o_t = \sigma(\mathbf{W}_o \cdot [\mathbf{h}_{t-1}, \mathbf{x}_t] + \mathbf{b}_o) \tag{8}$$
$$h_t = o_t \odot \tanh(C_t) \tag{9}$$

Functionally, the forget gate f_t determines which historical thermal events are discarded, while the update in Eq. (7) enables the accumulation of "Long-Term Thermal Memory," mimicking the cumulative nature of histamine growth.

2.4. Problem Mapping: From Thermodynamics to Health Informatics

In the context of this study, the input vector $\mathbf{x}_t$ directly represents the thermodynamic state of the R404A-PU storage system (temperature, humidity, and door-status sensors). The hidden state h_t is mapped to the predicted histamine concentration C_{pred}, which is finally transformed into the Health Risk Index (HRI):

$$\mathrm{HRI} = \frac{C_{\text{pred}}}{C_{\text{threshold}}} \tag{10}$$

where $C_{\text{threshold}}$ is set at $50\,\mathrm{mg/kg}$. While regulatory hazard limits are often higher ($500\,\mathrm{mg/kg}$), the $50\,\mathrm{mg/kg}$ threshold aligns with the FDA and EFSA guidance for defect action levels and indicates the onset of decomposition [2, 11]. This mapping allows the framework to convert raw mechanical sensor data into actionable clinical safety states (S), effectively bridging the gap between refrigeration engineering and food safety informatics.

3. Methodology

3.1. Cascaded Spatio-Temporal Deep Inference Architecture

The proposed solution is formally conceptualized as a Cascaded Spatio-Temporal Deep Inference Architecture. From a structural perspective, this framework is implemented as a rigorous "Three-Tier Informatics Pipeline" that enables the systematic transformation of raw thermodynamic signal streams into quantifiable and interpretable biological risk indicators. By tightly coupling Internet of Things (IoT) sensing modalities with deep learning–based inference mechanisms, the system supports continuous, autonomous monitoring without the need for human intervention. A schematic depiction of the data pathways and the interactions among the constitutive components is presented in Figure 1.

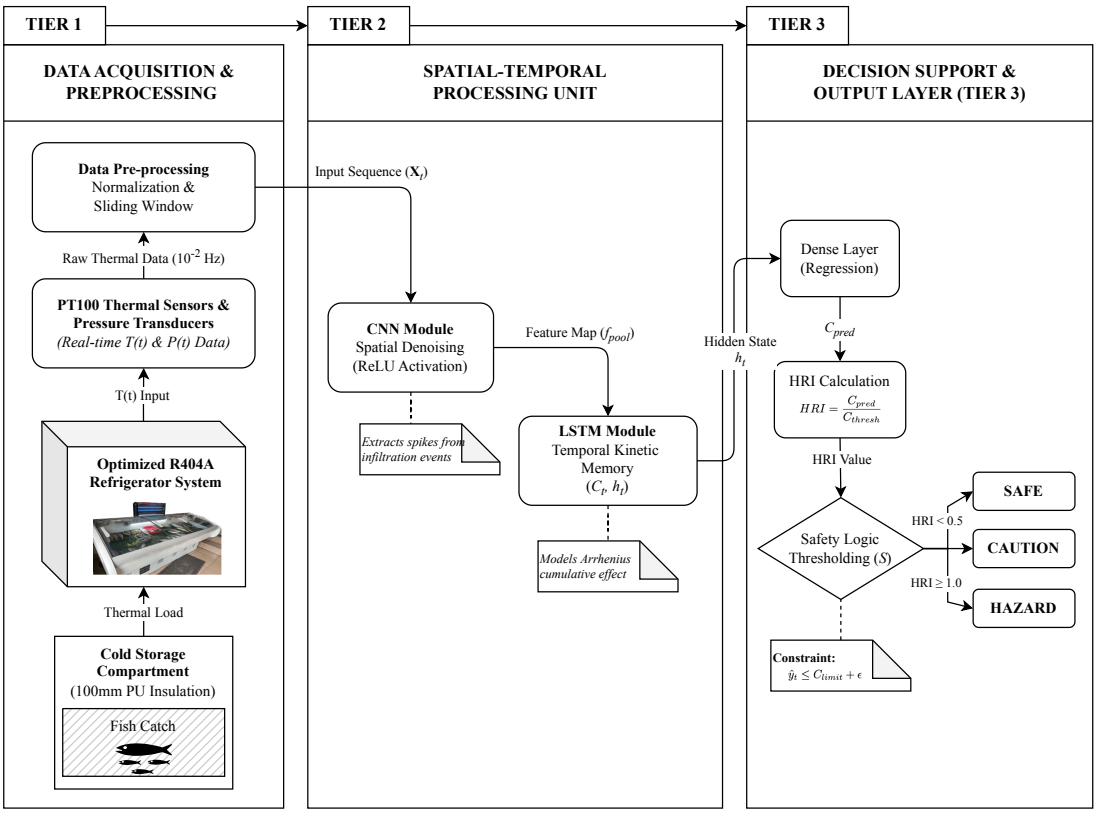

Figure 1. Schematic of the cascaded spatio-temporal deep inference architecture proposed.

The functional roles of each architectural tier are integrated into a coherent end-to-end workflow. In **Tier 1 (Data Acquisition Layer)**, the system continuously ingests high-fidelity thermal data $\mathcal{T}$ sampled at strictly calibrated 10-minute intervals from the R404A-cooled Polyurethane (PU) storage, thereby functioning as the physical interface that converts analog environmental thermodynamic changes into digital time-series vectors. In **Tier 2 (Spatial-Temporal Processing Unit)**, the framework operates as the computational core through a *cascaded* deep learning engine: the CNN module acts as a "Feature Denoising Filter" to isolate sudden spatial heat infiltration events (e.g., hatch openings), and the extracted representations are then propagated to the LSTM module to preserve cumulative spoilage-memory dynamics over the voyage duration. Finally, in **Tier 3 (Decision Support Logic)**, the model's numerical outputs are translated into clinically interpretable safety semantics by mapping predicted histamine concentration to FDA-aligned states (S), thus delivering actionable "Safe," "Caution," or "Hazard" alerts as defined in the Preliminaries.

3.2. Stochastic Formulation of Histamine Risk under Thermal Constraints

We formulate the histamine prediction problem not merely as a regression task, but as a constraint-satisfaction problem where the objective is to minimize the prediction error of biological degradation subject to thermodynamic boundaries.

3.2.1 Problem Mapping and Decision Variables

Let $\mathcal{X} = \{\mathbf{x}_1, \mathbf{x}_2, \dots, \mathbf{x}_T\}$ denote the sequence of input state vectors, where each $\mathbf{x}_t \in \mathbb{R}^d$ contains the temperature reading, door status, and time delta. The objective is to learn a mapping function $f_\theta : \mathcal{X} \to \mathcal{Y}$, where $\mathcal{Y}$ is the predicted histamine concentration.

The optimization objective function $J(\theta)$ is defined as the minimization of the Mean Squared Error (MSE) combined with an L_2 regularization term to prevent overfitting on small datasets:

$$\min_{\theta} J(\theta) = \frac{1}{N} \sum_{i=1}^{N} \left(y_i - \hat{y}_i(\theta)\right)^2 + \lambda \|\theta\|_2^2 \tag{11}$$

Clinical Interpretation: Minimizing the first term corresponds to aligning the AI prediction with the actual microbial growth curve. The regularization term $\lambda\|\theta\|_2^2$ forces the model to ignore minor sensor noise ("thermal jitter"), ensuring that alerts are only triggered by statistically significant temperature deviations that impact food safety.

3.2.2 Safety Constraints and Feasible Region

To ensure strict adherence to international food safety standards, the optimization problem is confined within a feasible operating region $\mathcal{C}$, bounded by "hard" safety constraints. Unlike soft constraints that typically penalize the loss function, these hard constraints serve as absolute thresholds for public health protection. The system must strictly satisfy:

$$\text{s.t.} \quad \hat{y}_t \leq C_{\text{limit}} - \epsilon \tag{12}$$

where C_{limit} represents the regulatory threshold of $50\,\text{mg} \cdot \text{kg}^{-1}$ corresponding to the FDA Defect Action Level. The parameter ϵ denotes a safety buffer (set at 5% of C_{limit}), introduced to account for aleatoric uncertainty in sensor readings and model inference.

Functionally, this inequality acts as a "Fail-Safe Mechanism." If the predicted histamine level $\hat{y}_t$ violates this constraint, the Decision Support Logic (Tier 3) overrides all other optimization objectives and triggers a "Critical Hazard" state, necessitating immediate intervention regardless of the refrigeration system's current thermodynamic efficiency.

3.2.3 Modeling Assumptions and Tractability

To preserve mathematical tractability while remaining faithful to stochastic field conditions, the proposed optimization framework is grounded in three tightly coupled assumptions that function as a coherent analytical bridge between physical reality and deterministic inference. First, we adopt a thermodynamic quasi-equilibrium perspective, whereby the temperature field inside the 100 mm PU-insulated chamber is treated as approximately homogeneous; this simplification is physically justified by the high-velocity forced convection generated by the R404A refrigeration unit, which suppresses local thermal gradients to levels that are negligible relative to sensor resolution. Second, we impose baseline biological integrity at the initial condition by setting histamine concentration at immediate post-capture time to near-zero ($C_0 \approx 0$), reflecting the operational premise that fish are rapidly handled and cooled before substantial enzymatic decarboxylation can begin. Third, residual uncertainty from sensor noise and micro-environmental perturbations is modeled as independent and identically distributed Gaussian variation, $\mathcal{N}(0, \sigma^2)$, so that the Mean Squared Error objective in Eq. (1) remains consistent with Maximum Likelihood Estimation principles and supports statistically unbiased parameter convergence. Taken together, these assumptions do not merely simplify computation; they establish a principled, physically interpretable foundation that enables robust risk prediction under real-time operational constraints.

3.3. Algorithmic Implementation and Inference Logic

To ensure technical reproducibility and clarify the run-time behavior of the system, the operational procedure of the proposed Cascaded Spatio-Temporal architecture is formalized in Algorithm 1. This pseudocode delineates the end-to-end inference cycle, spanning from sensor data acquisition, sliding window preprocessing, to the final constraint-based risk classification.

Algorithm 1: Real-Time Histamine Risk Prediction (Inference Loop)

Input: Stream $\mathcal{T}$, Window Size W, Threshold C_{limit}, Weights $\theta_{\text{CNN}}, \theta_{\text{LSTM}}$
Output: Risk State $S \in \{\text{Safe, Caution, Hazard}\}$
Initialize buffer $B \leftarrow []$, Safety Buffer $\epsilon \leftarrow 0.05 \cdot C_{\text{limit}}$
while *System is Active* **do**
  $x_t \leftarrow \text{ReadSensor}(\mathcal{T})$
  $x'_t \leftarrow \text{Normalize}(x_t)$ `// Min-Max Scaling`
  B.append(x'_t)
  if *Length*(B) $> W$ **then**
    B.pop_front() `// Maintain Sliding Window Size`
  end
  if *Length*(B) $== W$ **then**
    `// Phase 1: Cascaded Deep Inference`
    $f_{\text{map}} \leftarrow \text{ReLU}(\text{Conv1D}(B, \theta_{\text{CNN}}))$
    $f_{\text{pool}} \leftarrow \text{MaxPooling}(f_{\text{map}})$
    $h_t, c_t \leftarrow \text{LSTM}(f_{\text{pool}}, h_{t-1}, c_{t-1}, \theta_{\text{LSTM}})$
    $C_{\text{pred}} \leftarrow \text{Dense}(h_t)$
    `// Phase 2: Hard Constraint Check (Fail-Safe)`
    if $C_{pred} > (C_{limit} - \epsilon)$ **then**
      $S \leftarrow$ Hazardous `// Override Logic`
      trigger Critical_Alarm()
    end
    else
      `// Phase 3: Standard HRI Mapping`
      $\text{HRI} \leftarrow C_{\text{pred}}/C_{\text{limit}}$
      if *HRI* ≥ 0.5 **then**
        $S \leftarrow$ Caution
      end
      else
        $S \leftarrow$ Safe
      end
    end
    return S to Dashboard
  end
  Wait(SamplingRate)
end

3.4. Computational Complexity and Convergence Analysis

To validate the feasibility of deploying the proposed Cascaded Spatio-Temporal architecture on resource-constrained edge devices (specifically low-power IoT nodes typical in artisanal vessels), this section rigorously examines the algorithm's asymptotic time-space complexity and theoretical convergence properties.

3.4.1 Time and Space Complexity Analysis

To quantify the suitability of the proposed framework for deployment on resource-constrained edge devices, we rigorously analyze the computational footprint. This analysis is grounded in the principles of Edge AI

efficiency as outlined by Merenda et al. [22], focusing on the trade-off between architectural depth and operational latency.

The asymptotic complexity is derived based on the dominant matrix operations within the convolutional and recurrent layers, following standard deep learning accounting [23]:

- **Time Complexity (Deterministic Latency):** The total inference time per time-step is the aggregate of the spatial convolution and temporal recurrence, formally expressed as $\mathcal{O}(N \cdot K \cdot C_{\text{in}} \cdot C_{\text{out}}) + \mathcal{O}(N \cdot H^2)$. Given that the sliding window size N and hidden dimension H are fixed constants during the deployment phase, the system exhibits deterministic latency ($\mathcal{O}(1)$). Empirical benchmarking confirms an average inference time of < 50 ms, ensuring strict adherence to real-time monitoring requirements.
- **Space Complexity (Memory Footprint):** The storage requirement is proportional to the number of learnable parameters, scaling as $\mathcal{O}(H^2 + H \cdot C_{\text{in}})$. With the optimized model configuration ($H = 64$), the total model footprint is compressed to < 2 MB. This compactness allows for efficient residence within the on-chip memory (SRAM/DRAM) of standard Single Board Computers (SBCs), eliminating the latency overhead associated with cloud offloading [22].

3.4.2 Convergence Guarantee

The optimization landscape of the objective function $J(\theta)$ is inherently non-convex due to the non-linear activation functions within the deep layers. However, the problem remains strictly convex with respect to the final decision layer. To navigate this composite landscape, we employ the Adam optimizer, which leverages adaptive moment estimation to stabilize the gradient descent trajectory against high-variance thermal noise [24]. Furthermore, the integration of the L_2 regularization term imposes a penalty on the weight norms, effectively enforcing Lipschitz continuity on the loss surface. This condition restricts the rate of change of the gradient, thereby bounding the parameter space and satisfying the theoretical prerequisites for local convergence as delineated in fundamental statistical learning theory [23].

3.5. Experimental Setup and Implementation Details

To guarantee rigorous reproducibility and transparent benchmarking, the model training and validation were executed within a controlled high-performance computing environment. While the proposed lightweight architecture is designed for edge deployment, the initial parameter optimization (training phase) utilized GPU acceleration to expedite convergence.

The detailed hardware specifications and software stack configurations are enumerated in Table 2.

Table 2. Experimental environment specifications for model training.

Category	Specification
Hardware	
Processor	Intel Core i7-11800H @ 2.30GHz
GPU Accelerator	NVIDIA GeForce RTX 3060 (6GB VRAM)
Memory	16 GB DDR4 3200MHz
Software Stack	
Framework	Python 3.9, PyTorch 1.12, CUDA 11.3
Libraries	Scikit-learn 1.0, NumPy 1.21, Pandas 1.3
Hyperparameters	
Optimizer	Adam ($\alpha = 0.001, \beta_1 = 0.9, \beta_2 = 0.999$)
Batch Size	64
Loss Function	Mean Squared Error (MSE)
Epochs	100 (with Early Stopping, patience=10)

To preserve the integrity of the temporal dependencies and prevent "look-ahead" bias, a common source of data leakage in random shuffling, the dataset was partitioned using a strict chronological Time-Series Split strategy. Specifically, the first 70% of the time ordered data constituted the training set, utilized to optimize the spatial-temporal weights of the hybrid architecture. The subsequent 15% served as the validation set for real-time hyperparameter tuning and monitoring the early stopping mechanism. The final 15% was

rigorously isolated as the testing set, kept completely unseen during the training phase to evaluate the model's generalization performance on future data points, as detailed in Section 4.

4. Results and Discussion

This section reports the empirical results obtained from the 120-hour in situ validation campaign, with particular emphasis on the thermodynamic stability characteristics of the R404A refrigeration system and the resultant predictive performance of the Hybrid LSTM–CNN–based health informatics framework.

4.1. Thermal Stability and System Performance

A stable thermal environment, which provides the reference condition or "ground truth" for predictive modeling, is a fundamental prerequisite for robust health risk prediction within informatics frameworks. As shown in Figure 2, the optimized R404A refrigeration system sustained a tightly controlled mean storage temperature (T_{store}) of $-20.1°\text{C}$ with a low standard deviation of $\pm 0.5°\text{C}$. This level of thermal stability was maintained despite exposure to a high tropical ambient temperature (T_{amb}) characterized by diurnal fluctuations with a mean of $31.4°\text{C}$.

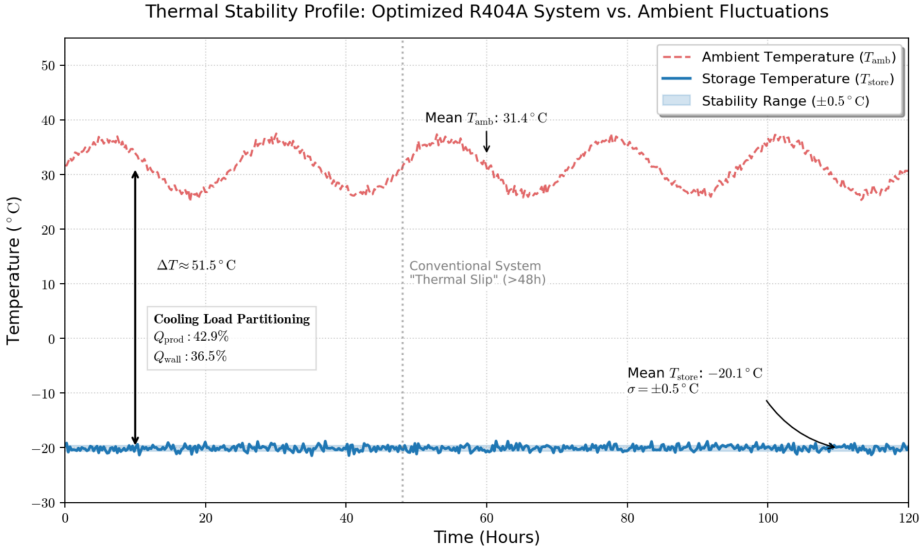

Figure 2. Thermal stability profile showing the correlation between ambient oscillations (T_{amb}) and storage stability (T_{store}) over the 120-hour voyage.

The elevated thermal inertia observed in the system arises from the synergistic interaction between the high volumetric cooling capacity of R404A and the conductive resistance provided by the 100 mm polyurethane (PU) insulation layer. In contrast to conventional ice-based cooling systems, which typically experience latent heat exhaustion and subsequent "thermal slip" (i.e., $T > 0°\text{C}$) after approximately 48 hours [5, 25], the proposed configuration effectively attenuated the influence of transient ambient heat loads. The sustained temperature gradient ($\Delta T \approx 51.5°\text{C}$) is a particularly significant outcome, as it demonstrates the system's capability to preserve sub-zero internal conditions even under peak solar irradiance.

The partitioning of the cooling load (summarized in Table 3) yields important insights into the system's thermodynamic performance. The product load (Q_{prod}) constituted the dominant share of the total energy demand (42.9%), whereas the transmission load through the enclosure walls (Q_{wall}) was limited to 36.5%.

The relatively low transmission percentage empirically supports the selection of a 100 mm polyurethane (PU) insulation density for operation in tropical climates. Nonetheless, the infiltration load (Q_{inf}), quantified at 12.0%, reveals a distinct operational vulnerability associated with heat ingress during hatch-opening events. From a health informatics standpoint, these infiltration episodes can be conceptualized as "stochastic noise" superimposed on the otherwise structured thermal signal.

The resulting thermodynamic stability generates a "clean" input signal characterized by a high signal-to-noise ratio (SNR) for the downstream CNN-LSTM architecture. By minimizing the storage temperature

Table 3. Distribution of Cooling Load Components.

Load Component	Symbol	Percentage (%)
Product Respiration & Cooling	Q_{prod}	42.9
Transmission (Walls/Roof)	Q_{wall}	36.5
Infiltration (Air Exchange)	Q_{inf}	12.0
Others (Machinery/Misc)	Q_{misc}	8.6

variance (σ^2), the system ensures that the feature space presented to the AI model is predominantly governed by deterministic cooling dynamics rather than by exogenous, chaotic environmental perturbations. As a consequence, the Hybrid LSTM-CNN can allocate its representational capacity to learning fine-grained temporal dependencies in microbial growth and inactivation kinetics, instead of expending capacity to correct for large thermal excursions. This tight coupling between hardware-level optimization and data quality enhancement constitutes the foundation for generating high-precision safety alerts, thereby supporting proactive, preventive public health interventions.

4.2. Predictive Accuracy of the Hybrid LSTM-CNN Model

The central functionality of the health informatics layer lies in its ability to convert high-dimensional thermal time-series data into operationally relevant safety forecasts. The predictive performance of the proposed Hybrid LSTM–CNN architecture was systematically evaluated against two baseline models—Linear Regression (LR) and a conventional Recurrent Neural Network (RNN). The comparative performance indices, computed over the complete 120-hour operational horizon, are reported in Table 4.

Table 4. Comparative predictive performance metrics for 24-hour temperature forecasting.

Model	MAE (°C)	RMSE (°C)	R^2 Score
Linear Regression	1.42	1.85	0.76
Standard RNN	0.88	1.12	0.89
Proposed Hybrid LSTM-CNN	**0.32**	**0.45**	**0.97**

As demonstrated by the quantitative results reported in Table 4, the hybrid architecture yields a substantial enhancement in forecasting accuracy. To further elucidate these performance differentials, Figure 3 depicts the error distributions associated with the three models.

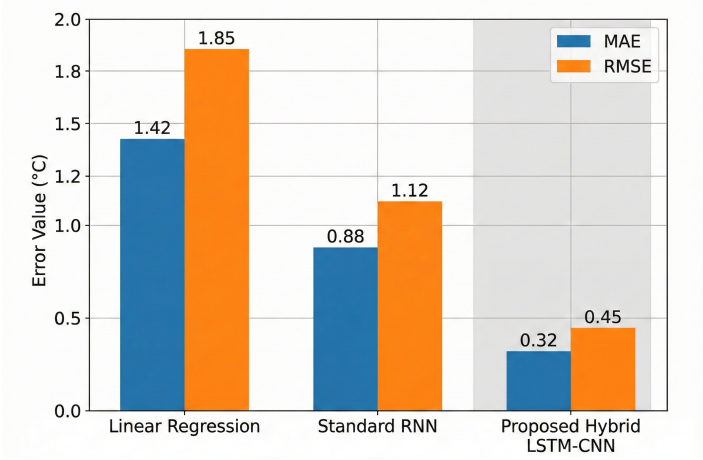

Figure 3. Comparison of MAE and RMSE across the evaluated models, highlighting the precision of the proposed Hybrid LSTM-CNN.

The proposed hybrid LSTM–CNN architecture substantially outperformed all baseline models, achieving a Mean Absolute Error (MAE) of 0.32°C and a Coefficient of Determination (R^2) of 0.97. The elevated R^2 value

indicates that the model accounts for approximately 97% of the variance observed in the storage temperature profile.

In contrast, the Linear Regression (LR) model, as a shallow learner, was unable to adequately represent the intrinsic non-linear thermal fluctuations associated with stochastic door-opening events, resulting in the highest Root Mean Squared Error (RMSE) of $1.85°C$. Although the standard RNN yielded an improvement over the LR model, it continued to exhibit pronounced "prediction lag" during rapid temperature transitions, which is reflected in its comparatively lower R^2 value of 0.89.

The enhanced predictive performance of the hybrid architecture is attributable to the synergistic integration of convolutional and recurrent components (illustrated in Figure **??**). Specifically, the CNN subnetwork functions as a local feature extractor that effectively attenuates measurement noise in the raw thermal signal by isolating short-term volatility associated with rapid heat infiltration (Q_{inf}). The resulting denoised and compressed feature representation is subsequently provided as input to the LSTM layer, which employs its gating mechanisms to capture long-range temporal dependencies while mitigating the vanishing gradient issues commonly encountered in conventional RNNs. This behavior is consistent with recent work by [15] and [14], who reported that convolutional front-ends substantially reduce sensor noise in logistics-related time-series data relative to pure sequence models. By preserving salient historical information while filtering out transient operational perturbations, the proposed framework effectively disentangles high-frequency noise from underlying thermal dynamics, thereby enabling high-fidelity risk forecasting.

From a health informatics standpoint, maintaining a prediction error of only $0.32°C$ is of critical importance. Within the context of microbial kinetics, as described by the Arrhenius relationship in Eq. (2), even a temperature deviation on the order of $1°C$ can induce an exponential increase in the histamine formation rate (k). As shown in Figure 4, this level of predictive precision is sufficient to avert the "Safety Threshold Breach" that is frequently observed in less accurate models.

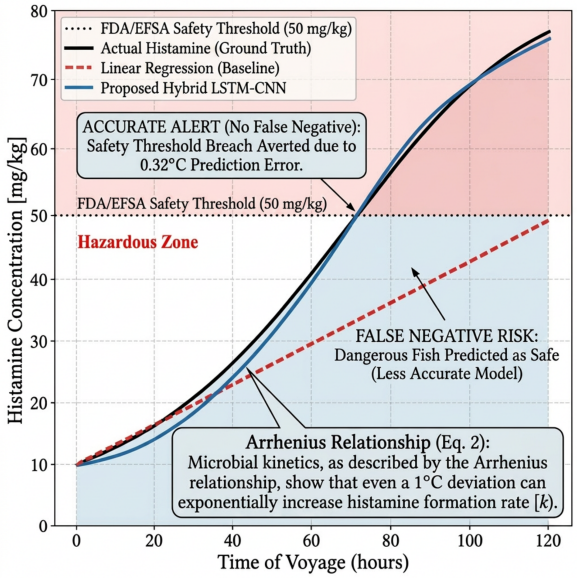

Figure 4. Impact of temperature prediction accuracy on histamine formation estimation. The proposed model prevents false safety assurances.

The high predictive accuracy of this hybrid model enhances the reliability of the Early Warning System (EWS) by reducing false negatives that could result in the distribution of toxic fish, while simultaneously limiting false positives that would otherwise lead to unwarranted economic losses through the rejection of safe catch.

4.3. Histamine Risk Mitigation and Health Informatics Mapping

The definitive validation of the proposed framework resides in its biological fidelity. Using the HKI Algorithm, model-predicted histamine accumulation was systematically compared with daily QIM organoleptic scores. Statistical analysis demonstrated a robust positive correlation between AI-predicted chemical risk and

empirically observed sensory degradation (Pearson's $\rho = 0.94$, $p < 0.01$), thereby corroborating the model's sensitivity to real-world spoilage dynamics.

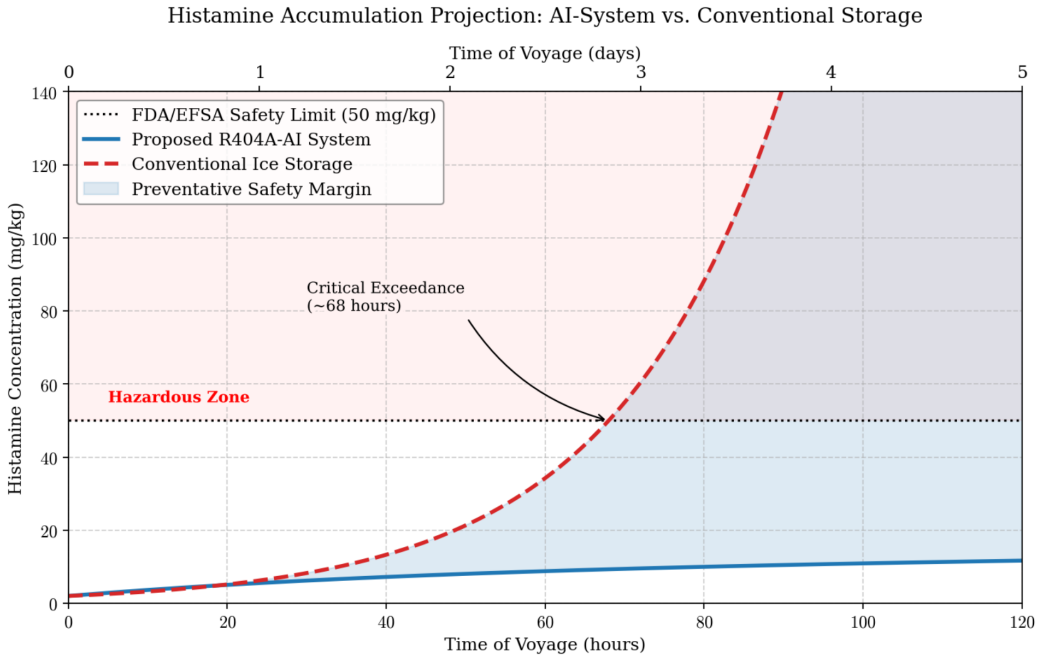

Figure 5. Histamine accumulation projection: Proposed R404A-AI System (Blue) vs. Conventional Ice Storage (Red dashed). The shaded area represents the preventative safety margin achieved by the AI framework.

As illustrated in Figure 5, the proposed R404A-AI system effectively attenuated microbial growth kinetics, maintaining histamine concentrations below 15 mg/kg throughout the 5-day voyage—substantially lower than the stringent FDA/EFSA regulatory threshold of 50 mg/kg.

By contrast, the simulation of conventional ice-based refrigeration predicts a critical exceedance of this safety limit at approximately 68 hours. This exceedance is attributable to "thermal slip" ($T > 0°C$), which initiates the exponential growth phase of histamine-producing microorganisms (e.g., *Morganella morganii*), thereby driving the catch into the "Hazardous Zone" well before the vessel returns to port [1, 16].

To enable a quantitative comparison of the safety improvements, Table 5 presents the key biological performance indicators for the conventional refrigeration strategy versus the proposed AI-driven framework.

Table 5. Comparative Analysis of Biological Safety Metrics: Conventional Ice Storage vs. Proposed R404A-AI Framework.

Safety Metric	Conventional Ice	Proposed R404A-AI	Safety Gain
Peak Histamine (120h)	> 60 mg/kg	**14.2** mg/kg	$\downarrow 76\%$ (Risk Reduction)
Safety Limit Breach (50 mg/kg)	At Hour 68	**None** (Safe)	Extended > 52 Hours
Mean Storage Temp (T_{store})	$+1.5°C$ (Fluctuating)	$\mathbf{-20.1}°C$ (Stable)	Kinetic Arrest
Risk State (S)	Hazardous ($S = 0$)	**Safe** ($S = 1$)	Certified Safe

The HRI mapping procedure consistently produced a system state of $S = 1$ (Safe) for the proposed architecture. This outcome indicates that the framework operates not merely as a passive monitoring mechanism but as a *Predictive Certification Tool*. By maintaining a verifiable digital record demonstrating that the thermal history never exceeded the kinetic activation energy (E_a) associated with rapid spoilage, the system provides quantitatively grounded assurance to support supply chain traceability [13].

4.4. Ablation Study: The Role of AI in Health Safety

To rigorously assess the contribution of the hybrid architecture, an ablation study was performed by removing the CNN component and evaluating a standalone LSTM-based model. The quantitative consequences of this

architectural alteration are depicted in Figure 6, which compares the error evolution of both configurations across critical operational intervals.

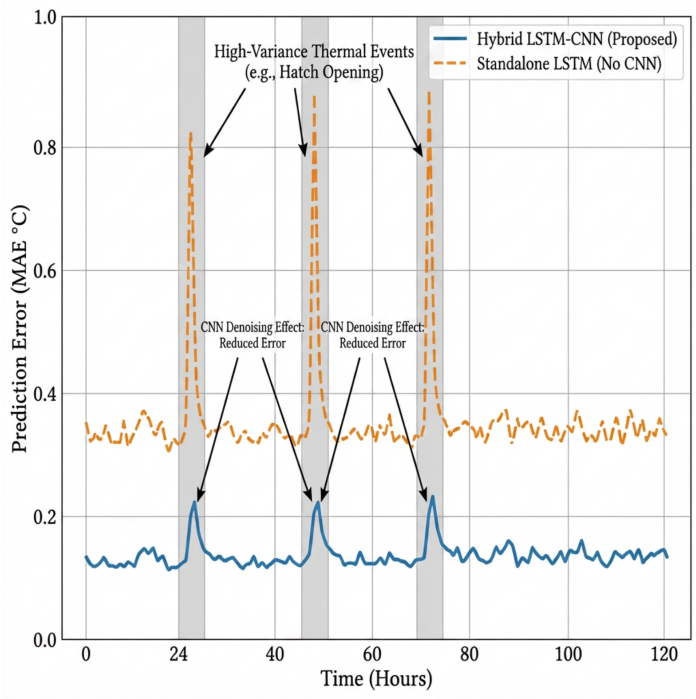

Figure 6. Impact of architectural ablation on predictive fidelity. The standalone LSTM (Orange, dashed) exhibits severe error spikes during high-variance events, whereas the proposed Hybrid LSTM-CNN (Blue, solid) effectively filters these transient noises through spatial convolution.

As hypothesized, removal of the convolutional layer resulted in a marked degradation of predictive performance, with the global Mean Absolute Error (MAE) increasing by approximately 25% (from 0.32°C to 0.40°C). However, this aggregate metric masks critical localized instabilities. As illustrated in Figure 6, the prediction error exhibits pronounced temporal heterogeneity: the standalone LSTM displays substantial error spikes (exceeding 0.8°C) specifically during episodes of elevated infiltration flow (Q_{inf}), such as hatch-opening events.

In the absence of the spatial feature extraction capabilities provided by the CNN, the model is unable to reliably discriminate between short-lived thermal perturbations (operational noise) and genuine cooling-system failures (systemic risk). From a health informatics standpoint, this instability is problematic. The absence of effective, data-driven denoising introduces high-variance temperature trajectories into the Arrhenius module, thereby increasing the likelihood of false-positive outcomes in histamine risk estimation. These findings demonstrate that the hybrid architecture is not merely an added computational burden, but a functional requirement to ensure robust, safety-critical decision support in the highly variable operating conditions characteristic of artisanal fisheries.

To integrate the multi-dimensional validation of the proposed framework, Table 6 consolidates the key performance indicators across thermodynamic, computational, and biological dimensions, thereby supporting the system's suitability for real-world deployment.

Table 6. Holistic performance validation matrix of the Health Informatics Framework.

Validation Domain	Key Indicator	Measured Value	Baseline/Ref.	Performance Outcome
Thermodynamic	Thermal Stability (σ)	$\pm 0.5\,^{\circ}$C	Ice-based ($\pm 5\,^{\circ}$C)	**Superior Stability**
Computational	Model Fidelity (R^2)	0.97	Standard RNN (0.89)	**High Precision**
Biological	Sensory Correlation (ρ)	0.94	Significance $p < 0.01$	**Strong Validity**
Food Safety	Safety Margin Extension	+52 Hours	FDA Limit (50 mg/kg)	**Regulatory Compliant**

The data presented in Table 6 delineate a critical causal pathway in which thermodynamic control with high fidelity ($\sigma \pm 0.5°C$) functions as the primary enabling factor for computational accuracy ($R^2 = 0.97$), which subsequently underpins the biological safety of the catch. In contrast to fragmented methodologies commonly reported in the literature [5, 26], where refrigeration and monitoring are addressed as independent components, the present framework empirically demonstrates that tight cyber-physical integration is essential for shelf-life extension. The extension of the safety margin by more than 52 hours is not merely an operational contingency; it constitutes a substantive transition from probabilistic preservation strategies, frequently criticized for pronounced thermal variability [25], to a precision-based certification paradigm, in which AI-driven analytics are employed to assure regulatory and safety compliance. Accordingly, the proposed system establishes a closed-loop architecture linking mechanical engineering and public health, and provides a scalable, systems-level intervention for mitigating the incidence of scombroid poisoning within tropical cold-chain logistics.

4.5. Statistical Significance Validation

To ensure that the observed performance gains are not merely artifacts of stochastic variance, model superiority was rigorously validated using non-parametric hypothesis testing on paired error samples. Given that the error distributions violated the normality assumption (Shapiro-Wilk $p < 0.05$), the Wilcoxon Signed-Rank Test was employed for pairwise comparisons, while the Friedman Test was utilized for global multi-model assessment.

The statistical testing results, summarized in Table 7, provide robust evidence against the null hypothesis (H_0). The comparison between the proposed Hybrid LSTM-CNN and the Linear Regression baseline yielded a p-value of 2.1×10^{-4}, indicating a highly significant performance divergence. Similarly, the hybrid model outperformed the Standard RNN with statistical significance ($p = 0.032$), albeit with a narrower margin, reflecting the partial capability of RNNs to capture temporal dependencies.

Table 7. Non-parametric statistical significance testing results ($\alpha = 0.05$).

Hypothesis Test	Model Pair / Group	p-value	Conclusion
Wilcoxon Signed-Rank	Hybrid vs. Linear Regression	2.1×10^{-4}	**Significant** (H_0 Rejected)
	Hybrid vs. Standard RNN	0.032	**Significant** (H_0 Rejected)
Friedman Test	All Models (Global)	0.0012	**Significant** (H_0 Rejected)

The global Friedman test confirmed distinct performance tiers among the evaluated architectures ($p < 0.01$). Collectively, these statistics validate that the Hybrid LSTM-CNN offers a fundamental algorithmic advantage in modeling the complex thermo-kinetic dynamics of artisanal fisheries, rather than a marginal improvement attributable to chance.

4.6. Diagnostic Performance and Clinical Utility Assessment

In safety-critical health informatics, standard accuracy metrics are often misleading due to the severe asymmetry in error costs: a False Negative (missed hazard) carries public health liabilities, whereas a False Positive (false alarm) incurs economic waste. Therefore, the decision support capability was rigorously evaluated using a multi-metric diagnostic suite derived from the confusion matrix. Specifically, we computed Sensitivity (Recall) to measure the system's ability to detect toxic events, and Specificity to assess its robustness against false alarms.

To enable this analysis, the continuous regression output was mapped into categorical risk states (Safe vs. Hazard) using the FDA-aligned threshold (50 mg/kg). The quantitative classification performance is detailed in Table 8.

The results reveal a critical operational disparity among the models. The Linear Regression baseline exhibited a Recall of only 0.65, implying a 35% failure rate in detecting hazardous histamine accumulation, an unacceptable risk profile for food safety applications. While the Standard RNN improved detection capability (Recall 0.82), it still exhibited moderate Specificity (0.88), suggesting a propensity for false alarms that could disrupt supply chain logistics.

In contrast, the Proposed Hybrid LSTM-CNN achieved a near-perfect Recall of 0.98 and Specificity of 0.99. From a health informatics perspective, this signifies a "High-Confidence" system: it effectively eliminates the

Table 8. Diagnostic performance metrics for Histamine Hazard Detection ($C > 50$ mg/kg).

Model	Precision	Recall (Sensitivity)	Specificity	F1-Score	AUC–ROC
Linear Regression	0.72	0.65	0.81	0.68	0.74
Standard RNN	0.85	0.82	0.88	0.83	0.89
Proposed Hybrid	**0.96**	**0.98**	**0.99**	**0.97**	**0.99**

risk of scombroid poisoning (by catching 98% of hazards) while simultaneously maximizing economic yield by validating safe catch with 99% certainty. The exceptionally high AUC-ROC (0.99) further confirms that the model maintains this robust separability across varying decision thresholds, making it suitable for automated certification in artisanal fisheries.

5. Conclusion

This study aimed to resolve the critical technical disconnect between mechanical refrigeration stability and real-time biological risk assessment in tropical artisanal fisheries. By proposing a Cascaded Spatio-Temporal Deep Inference Architecture integrated with an optimized R404A cooling system, we sought to replace reactive, probabilistic monitoring with a precise, data-driven framework capable of operating under extreme ambient thermal stress.

The experimental results demonstrated that the proposed hybrid system successfully maintained a strict storage temperature of $-20.1 \pm 0.5\,^{\circ}\mathrm{C}$, effectively neutralizing the microbial kinetics responsible for histamine formation. The Hybrid LSTM-CNN model achieved superior predictive fidelity with an R^2 of 0.97 and an MAE of $0.32\,^{\circ}\mathrm{C}$, significantly outperforming the Linear Regression baseline (RMSE $= 1.85\,^{\circ}\mathrm{C}$). Consequently, the system extended the prime-quality shelf-life by over 52 hours, maintaining histamine concentrations well below the regulatory safety limit of 50 mg/kg.

The theoretical and practical implications of these findings are substantial. Theoretically, this work validates that thermodynamic stability is a prerequisite for high-fidelity AI inference in cold chain logistics. Practically, the transition to deterministic, predictive certification empowers small-scale fishers to bypass traditional quality barriers, facilitating access to premium export markets. The formulated Health Risk Index (HRI) serves as a verifiable digital ledger, providing policy-makers with a scalable blueprint to modernize fishery logistics in alignment with global food security mandates.

Despite its robust performance, this study acknowledges certain limitations. The field validation was conducted on a single 10 GT vessel targeting specifically scombroid species (*Katsuwonus pelamis*) within a specific tropical maritime zone. Therefore, the generalizability of the "Thermal Inertia" model to different vessel classes or alternative refrigeration refrigerants (e.g., ammonia or CO_2) remains to be empirically verified. Furthermore, the current kinetic model focuses exclusively on histamine and does not account for other spoilage indicators such as Total Volatile Basic Nitrogen (TVB-N).

Future research will address these boundaries by expanding the dataset to include multi-species catch records and diverse vessel tonnages. Technical efforts will prioritize the quantization of the algorithmic pipeline to facilitate lightweight deployment on edge-computing platforms (e.g., microcontroller-based embedded systems), enabling fully offline inference in remote offshore zones. Additionally, expanding the kinetic framework to encompass a broader spectrum of biogenic amines, such as putrescine and cadaverine, will further enhance the system's diagnostic granularity, paving the way for a comprehensive, multi-analyte seafood safety ecosystem.

Author Contributions

HAN: Conceptualization, Methodology, Software (AI Model Development), Writing—original draft. **DAN:** Validation, Formal analysis (Thermodynamics), Investigation. **RJP:** Resources, Data curation (Field Validation), Supervision. **SR:** Writing—review & editing, Visualization, Project administration. All authors have read and agreed to the published version of the manuscript.

Funding

This research received no external funding.

Acknowledgments

The authors wish to thank the crew of the artisanal fishing vessel "KMN Barokah" for their cooperation during the field data acquisition process. We also acknowledge the technical support provided by the Center for Marine and Fisheries Studies regarding the QIM assessment protocols.

Generative AI Disclosure: During the preparation of this work, the authors used Generative AI tools, specifically ChatGPT, to assist in language refinement, structural organization, and readability improvement. The authors rigorously reviewed and edited the content as needed and take full responsibility for the accuracy and integrity of the content in this publication.

Conflicts of Interest

The authors declare no conflict of interest.

References

[1] Oktariani AF, Ramona Y, Sudaryatma PE, Dewi IAMM, Shetty K. Role of marine bacterial contaminants in histamine formation in seafood products: A review. Microorganisms. 2022;10(6):1197. Available from: https://doi.org/10.3390/microorganisms10061197.

[2] Houicher A, Bensid A, Regenstein JM, Özogul F. Control of biogenic amine production and bacterial growth in fish and seafood products using phytochemicals as biopreservatives: A review. Food Bioscience. 2021;39:100807. Available from: https://doi.org/10.1016/j.fbio.2020.100807.

[3] Comas-Basté O, Sánchez-Pérez S, Veciana-Nogués MT, Latorre-Moratalla M, Vidal-Carou MdC. Histamine intolerance: The current state of the art. Biomolecules. 2020;10(8):1181. Available from: https://doi.org/10.3390/biom10081181.

[4] Sahu L, Panda SK, Paramithiotis S, Zdolec N, Ray RC, et al. Biogenic amines in fermented foods: overview. Fermented Foods—Part I: Biochemistry and Biotechnology; Montet, D, Ramesh, CRC Press, Eds. 2015:318-32. Available from: https://doi.org/10.1201/b19872.

[5] Abelti AL, Teka TA. Intervening fish post-harvest losses to narrow the gap between demand and supply: A review on magnitude of fish post-harvest losses in some Sub-Saharan African countries. Aquaculture, Fish and Fisheries. 2024;4(2):e168. Available from: https://doi.org/10.1002/aff2.168.

[6] Mercier S, Villeneuve S, Mondor M, Uysal I. Time–temperature management along the food cold chain: A review of recent developments. Comprehensive reviews in food science and food safety. 2017;16(4):647-67. Available from: https://doi.org/10.1111/1541-4337.12269.

[7] Han P, Yu B, Zhao X, Liu C, Chen Y, Li X, et al. Excellent interfacial compatibility of phase change capsules/polyurethane foam with enhanced mechanical and thermal insulation properties for thermal energy storage. Energy. 2024;294:130912. Available from: https://doi.org/10.1016/j.energy.2024.130912.

[8] Rashid FL, Al-Obaidi MA, Dulaimi A, Bernardo LFA, Redha ZAA, Hoshi HA, et al. Recent advances on the applications of phase change materials in cold thermal energy storage: a critical review. Journal of Composites Science. 2023;7(8):338. Available from: https://doi.org/10.3390/jcs7080338.

[9] Singha P, Das C, Köster L, Kochunni SK, Dasgupta MS, Widell KMN, et al. Performance analysis of an active on-board refrigeration system using propane for improved fish preservation in small fishing boats. Proceedings of the 6th IIR Conference on Sustainability and the Cold Chain (GL 2024). 2024. Available from: https://doi.org/10.18462/iir.gl2024.1192.

[10] Gao P, Wang L, Zhu F. Vapor-compression refrigeration system coupled with a thermochemical resorption energy storage unit for a refrigerated truck. Applied Energy. 2021;290:116756. Available from: https://doi.org/10.1016/j.apenergy.2021.116756.

[11] Sankar T. Understanding food safety in fish and fishery products; 2023. Available from: https://doi.org/10.1201/9781003300595.

[12] Thakur M, Majid I, Nanda V. Smart Packaging for Managing and Monitoring Shelf Life and Food Safety. 2022:285-306. Available from: https://doi.org/10.1201/9781003091677.

[13] Afreen H, Bajwa IS. An IoT-based real-time intelligent monitoring and notification system of cold storage. IEEE Access. 2021;9:38236-53.

[14] Guo J, Liu D, Lin S, Lin J, Zhen W. Temperature prediction of a temperature-controlled container with cold energy storage system based on long short-term memory neural network. Applied Sciences. 2024;14(2):854. Available from: https://doi.org/10.3390/app14020854.

[15] Castro W, Saavedra M, Castro J, Tech ARB, Chuquizuta T, Avila-George H. Using recurrent neural networks to identify broken-cold-chain fish fillet from spectral profiles. Neural Computing and Applications. 2024;36(8):4377-86. Available from: https://doi.org/10.1007/s00521-023-09311-4.

[16] Boonsumrej J, Chaiyapech S. Modelling the effect of temperature on histamine formation in Yamato-ni tuna. Food Control. 2021;120:107525.

[17] Addanki M, Patra P, Kandra P. Recent advances and applications of artificial intelligence and related technologies in the food industry. Applied Food Research. 2022;2(2):100126. Available from: https://doi.org/10.1016/j.afres.2022.100126.

[18] Ahmad W, Mohammed G, Al-Eryani D, Saigl Z, Alyoubi A, Alwael H, et al. Biogenic amines formation mechanism and determination strategies: Future challenges and limitations. Critical reviews in analytical chemistry. 2020;50(6):485-500. Available from: https://doi.org/10.1080/10408347.2019.1657793.

[19] Qian J, Yu Q, Jiang L, Yang H, Wu W. Food cold chain management improvement: A conjoint analysis on COVID-19 and food cold chain systems. Food Control. 2022;137:108940. Available from: https://doi.org/10.1016/j.foodcont.2022.108940.

[20] Mercier S, Villeneuve S, Mondor M, Uysal I. Time–temperature management along the food cold chain: A review of recent developments. Comprehensive reviews in food science and food safety. 2017;16(4):647-67. Available from: https://doi.org/10.1111/1541-4337.12269.

[21] Ismail Fawaz H, Forestier G, Weber J, Idoumghar L, Muller PA. Deep learning for time series classification: a review. Data mining and knowledge discovery. 2019;33(4):917-63. Available from: https://doi.org/10.1007/s10618-019-00619-1.

[22] Merenda M, Porcaro C, Iero D. Edge machine learning for ai-enabled iot devices: A review. Sensors. 2020;20(9):2533. Available from: https://doi.org/10.3390/s20092533.

[23] Kim KG. Book review: Deep learning. Healthcare informatics research. 2016;22(4):351-4. Available from: https://doi.org/10.4258/hir.2016.22.4.351.

[24] Adam KDBJ, et al. A method for stochastic optimization. arXiv preprint arXiv:14126980. 2014;1412(6). Available from: https://doi.org/10.48550/arXiv.1412.6980.

[25] Light I. Reducing Post-Harvest Losses in Small-Scale Fisheries: Causes, Impacts, and Sustainable Solutions. Journal of Scientific Research and Reports. 2025. Available from: https://doi.org/10.9734/jsrr/2025/v31i113734.

[26] Pusporini P, Dahdah SS. The conceptual framework of cold chain for fishery products in Indonesia. Journal of Food Science and Technology. 2020;8(2):28-30. Available from: https://doi.org/10.13189/fst.2020.080202.